

# How to image a single protein

Jean-Nicolas Longchamp<sup>1,\*</sup>, Stephan Rauschenbach<sup>2</sup>, Sabine Abb<sup>2</sup>, Conrad Escher<sup>1</sup>, Tatiana Latychevskaia<sup>1</sup>, Klaus Kern<sup>2,3</sup>, Hans-Werner Fink<sup>1</sup>

<sup>1</sup>*Physics Department of the University of Zurich, Winterthurerstrasse 190, CH-8057 Zürich, Switzerland*

<sup>2</sup>*Max Planck Institute for Solid State Research, Heisenbergstrasse 1, DE-70569 Stuttgart, Germany*

<sup>3</sup>*Institut de Physique de la Matière Condensée, Ecole Polytechnique Fédérale de Lausanne, CH-1015 Lausanne, Switzerland*

\* Corresponding author: longchamp@physik.uzh.ch

**Imaging a single protein has been a long-standing dream for advancing structural biology and with this various fields in natural science. In particular, revealing the distinct conformations of an individual protein is of outermost importance. To do so, one needs to master and combine three requirements. At first, a method for isolating individual proteins for further inspection has to be at hand; quite the opposite to the current challenge of assembling proteins into a crystal for X-ray analysis<sup>1,2</sup>. Furthermore, technologies are required for keeping a single protein fixed in space long enough to accumulate sufficient structural information from a scattering experiment. Last but not least, gentle radiation with a wavelength small enough to uncover structural details while ensuring that radiation damage does not decompose the protein during observation as it is available by low-energy electron holography<sup>3</sup> is vital for imaging. Here we show that soft-landing electrospray beam deposition<sup>4,5</sup> allows for specific selection and sound deposition<sup>5</sup> of individual proteins and protein complexes onto ultraclean freestanding graphene<sup>6</sup> in an ultra-high vacuum environment. Due to the fact that graphene is transparent for low-energy electrons<sup>7</sup> and since the latter do not damage biological molecules<sup>8,9</sup>, we were able to acquire high signal-to-noise ratio electron holograms of individual proteins (Cytochrome C and BSA) as well as of protein complexes (haemoglobin). The numerical hologram reconstructions reveal the overall shape of single proteins. With this, images of individual folded proteins and protein complexes, not being the result of an averaging process, have been obtained for the first time.**

Most of the protein structural information available today has been obtained from either X-ray crystallography experiments or cryo-electron microscopy investigations by means of averaging over many molecules assembled into a crystal or over a large ensemble selected from low signal-to-noise ratio electron micrographs respectively<sup>10</sup>. Despite the impressive amount of available data, a strong desire for acquiring structural data from just one individual molecule is emerging for good reasons. Most of the biologically relevant molecules exhibit different conformations; the associated structural details however, remain undiscovered when averaging is involved. Moreover, a large subset of the entirety of proteins, in particular out of the important category of membrane proteins, does not crystallize at all. If just one individual protein or protein complex can be analysed in sufficient detail, also those objects become finally accessible.

For a meaningful contribution to structural biology, a tool for single molecule imaging has to allow for observing an individual protein long enough to acquire a sufficient amount of data for revealing its structure, ideally without destroying it. The strong inelastic scattering cross-section for both, X-rays and high-energy electrons as employed in the state-of-the-art aberration corrected TEMs, inhibits accumulation of sufficient elastic scattering events required in order to reveal high-resolution reconstruction of just one molecule. Future X-ray Free Electron Lasers (XFELs) with drastically enhanced brightness and reduced pulse duration might eventually achieve the goal of

single molecule imaging. Yet, the current and foreseeable state-of-the-art in XFEL performance still requires averaging over at least 1 million molecules<sup>1,11-13</sup>.

In contrast to this, biomolecules as for instance DNA withstand irradiation by low-energy electrons and remain unperturbed<sup>8,9</sup> even after a total dose of at least 5 orders of magnitude larger than the permissible dose in X-ray or high-energy electron imaging. While the damage-free radiation of low-energy electrons is appealing, a tool for single protein imaging critically relies on the sample preparation method. The protein has to be brought into an ultra-high vacuum (UHV) environment and fixed in space for an appropriate period of time for accumulating enough structural information on the one hand, while avoiding the emergence of contaminants on the other hand.

In the following, we show how by means of soft-landing electrospray ion beam deposition<sup>4,5</sup> (ES-IBD), individual native proteins<sup>14</sup> are transferred from aqueous solution to the gas phase to be deposited onto ultraclean freestanding graphene in a UHV environment for subsequent imaging by low-energy electron holography.

The workflow for imaging a single protein involves several steps as illustrated in Fig. 1. An ultraclean freestanding graphene sample is prepared using the recently developed platinum metal catalysis method<sup>6</sup> and characterized in the low-energy electron holographic microscope (Fig. 1 top). Such sample is subsequently transferred to an ES-IBD system (Fig. 1 middle) under permanent UHV conditions by means of a UHV suitcase operating in the  $10^{-11}$  mbar regime (see Supplementary Information for more details). Native cytochrome C (CytC), and haemoglobin (HG) ion beams are generated by electrospray ionization and mass filtering. For CytC the charge states  $z=5-7$  are selected<sup>15</sup>. In the case of HG the charge states  $z=16$  or  $z=17$  of the intact complex are known to be of native conformation<sup>16</sup> and hence the corresponding  $m/z$  region is selected (the corresponding mass spectra are displayed in the Supplementary Information). In a third experiment, bovine serum albumin (BSA) in the high-charge states  $z=35-60$  is chosen for deposition (see Extended Data Fig. 2). In all three cases, the ions land with a kinetic energy of 2-5eV per charge<sup>14</sup> on ultraclean freestanding graphene covering  $500 \times 500 \text{ nm}^2$  apertures milled in a 100nm thick SiN membrane<sup>6</sup>.

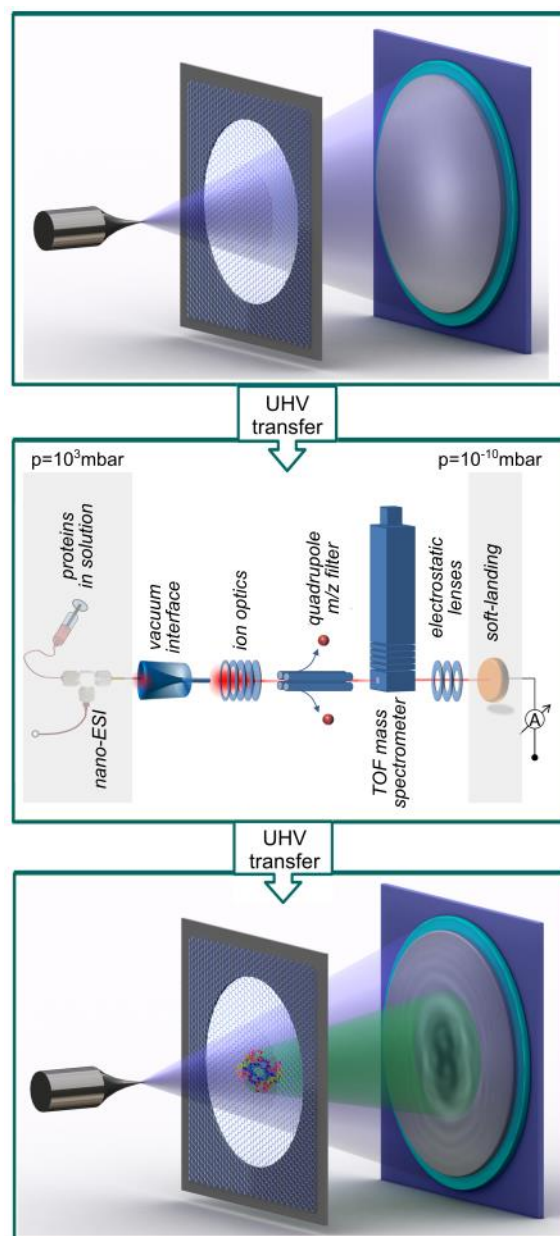


**Figure 1: Schematic workflow for imaging a single protein.** From top to bottom: Preparation and characterisation of ultraclean freestanding graphene. Deposition of proteins onto freestanding graphene in a  $m/z$  filtered ES-IBD system. Imaging of the proteins within the previously characterised region by means of low-energy electron holography. During the whole experimental workflow, the sample is kept under strict UHV conditions with the help of a UHV suitcase for the transfer between the two experimental chambers (see Supplementary Information for more details).

After deposition, the samples are transferred again under preserved UHV conditions from the ES-IBD system back to the low-energy electron holographic microscope, where low-energy electron holograms of individual proteins are recorded<sup>13</sup>. In this experimental scheme inspired by Dennis Gabor's original idea of holography, the samples are presented to a highly coherent beam of low-energy electrons generated by an atomically sharp field emitter tip placed as close as 100nm in front of the sample (Fig.1 bottom). The interference pattern formed by the scattered and the un-scattered electron waves, the so-called hologram, is recorded at a several centimetres distant electron detector (for more details see supplementary information). Subsequent numerical hologram reconstruction involving back propagation of the wave front from the hologram to the sample plane<sup>17-19</sup> finally reveals the protein structure.

Holograms of individual CytC proteins and their respective reconstructions are presented in Fig. 2(a-b). The shapes of the imaged proteins are compared with the structural data information obtained from X-ray crystallography investigations and available from the protein data bank (pdb id: 1HRC). The overall size of the imaged CytC corresponds to the expected dimensions and the low-energy electron images can be associated with proteins in several distinct orientations. The resolution in the electron images is sufficient to identify individual CytC as well as agglomerates thereof (Fig. 2b). As demonstrated previously with DNA<sup>8</sup>, no sign of decomposition of the protein during electron exposure is observed.

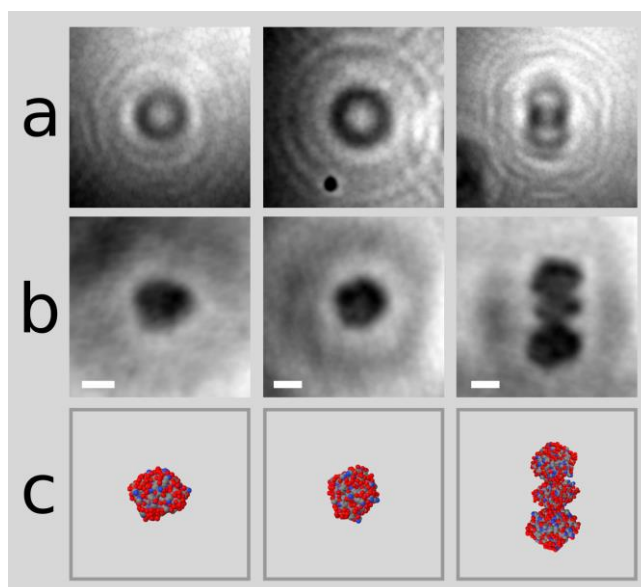


**Figure 2: Low-energy electron holograms of cytochrome C and their reconstructions.** *a*, Three holograms of CytC recorded at kinetic electron energies of 142eV (left), 132eV (middle), and 117eV (right). *b*, Numerical reconstructions showing the protein in different orientations on graphene. The scale bars correspond to 2nm. *c*, Suggestions for possible orientations based on the averaged protein structure derived from X-ray crystallography data and documented in the protein data bank (pdb id:1HRC). Survey images of freestanding graphene before and after deposition of CytC is presented in Extended Data Fig. 1.

From the data displayed in the right column of Fig. 2, it remains unsettled whether the agglomerate formed by several CytC has assembled prior or past deposition. On the other hand, in Fig. 3 two holograms and their respective reconstructions of individual haemoglobin are presented demonstrating that with our method it is not only possible to image individual proteins but also to deposit and image entire biologically relevant protein complexes. As apparent from the high contrast images of individual haemoglobin, not just the globular structure with the correct overall dimensions of the protein complex is revealed, but also details of its shape in different orientations. In Fig. 3(b right), structural features of 0.7-0.8nm in size can clearly be identified and may serve as a rough resolution estimate for the low-energy electron images. In a hologram the spacing between consecutive interference fringes gradually decreases towards higher orders. Hence, high-order interference fringes and consequently high-resolution structural details are most susceptible to mechanical vibrations. The latter are currently limiting the resolution and intense efforts are ongoing to increase the mechanical stability of the low-energy electron holographic microscope in order to overcome this limitation and approach atomic resolution.

At this stage, the comparison with the protein data bank structure has the character of a control experiment. However, the future goal is to directly uncover the structure of unknown proteins and all their possible conformations that might differ in the position of a small number of atoms only.

Nevertheless, on the road towards this ambition, additional fundamental questions remain to be addressed as for instance: the influence of the substrate, the possibility to add a hydration shell under UHV conditions, as well as issues related to transport, like diffusion of proteins and subsequent association into protein complexes. First observations of diffusion of folded proteins on freestanding graphene by means of low-energy electron holography are presented in the Extended Data Figure 3 illustrating that our method described here is also capable of accessing dynamical processes.

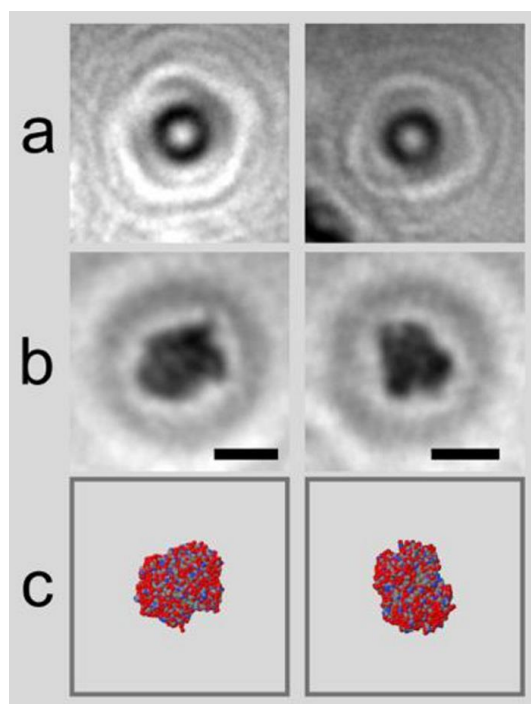


**Figure 3: Low-energy electron holograms of two individual haemoglobin and their reconstructions.** *a*, Two holograms of haemoglobin recorded at kinetic electron energies of 71eV (left) and 69eV (right) respectively. *b*, Numerical reconstructions showing the protein complex in two different orientations on graphene. The scale bars correspond to 5nm. The diffuse rings around the object are due to the presence of the out-of-focus twin image inherent to in-line holography. *c*, Suggestions for possible orientations based on the averaged protein structure derived from X-ray crystallography data and documented in the protein data bank (pdb id: 2QSS).

To conclude, we have shown how to image a single protein by combining the ES-IBD technology with low-energy electron holography. This has led to the first tool ever for revealing structural details of native single proteins and protein complexes without destroying them. With the recent advances in electrospray ionization of large protein complexes<sup>20</sup> and in particular membrane proteins<sup>21,22</sup>, even the structure of these biologically important but reluctant to readily crystallize entities will possibly become accessible in the near future.

While bare freestanding graphene has already been imaged with 2 Angstrom resolution by coherent diffraction with low-energy electrons<sup>23</sup>, it is now a challenge of adopting the technologies described here for reaching atomic resolution in structural biology at the single protein level.

## References:

1. Chapman, H. N. *et al.* Femtosecond X-ray protein nanocrystallography. *Nature* **470**, 73–77 (2011).
2. Caleman, C. *et al.* On the feasibility of nanocrystal imaging using intense and ultrashort X-ray pulses. *ACS Nano* **5**, 139–46 (2011).
3. Fink, H.-W., Stocker, W. & Schmid, H. Holography with low-energy electrons. *Phys. Rev. Lett.* **65**, 1204–1206 (1990).
4. Rauschenbach, S. *et al.* Electrospray Ion Beam Deposition of Clusters and Biomolecules. *Small* **2**, 540–547 (2006).
5. Rauschenbach, S. *et al.* Electrospray Ion Beam Deposition: Soft-Landing and Fragmentation of Functional Molecules at Solid Surfaces. *ACS Nano* **3**, 2901–2910 (2009).
6. Longchamp, J.-N., Escher, C. & Fink, H.-W. Ultraclean freestanding graphene by platinum-metal catalysis. *J. Vac. Sci. Technol. B Microelectron. Nanom. Struct.* **31**, 020605 (2013).
7. Longchamp, J.-N., Latychevskaia, T., Escher, C. & Fink, H.-W. Low-energy electron transmission imaging of clusters on free-standing graphene. *Appl. Phys. Lett.* **101**, 113117 (2012).
8. Germann, M., Latychevskaia, T., Escher, C. & Fink, H.-W. Nondestructive imaging of individual biomolecules. *Phys. Rev. Lett.* **104**, 095501 (2010).
9. Longchamp, J.-N., Latychevskaia, T., Escher, C. & Fink, H.-W. Non-destructive imaging of an individual protein. *Appl. Phys. Lett.* **101**, 93701 (2012).
10. Callaway, E. The revolution will not be crystallized: a new method sweeps through structural biology. *Nature* **525**, 172–174 (2015).
11. Neutze, R., Wouts, R., van der Spoel, D., Weckert, E. & Hajdu, J. Potential for biomolecular imaging with femtosecond X-ray pulses. *Nature* **406**, 752–757 (2000).
12. Miao, J. W., Sandberg, R. L. & Song, C. Y. Coherent X-ray diffraction imaging. *IEEE J. Sel. Top. Quantum Electron.* **18**, 399–410 (2012).
13. Miao, J. W., Hodgson, K. O. & Sayre, D. An approach to three-dimensional structures of biomolecules by using single-molecule diffraction images. *Proc. Natl. Acad. Sci. U. S. A.* **98**, 6641–6645 (2001).
14. Deng, Z. *et al.* A close look at proteins: submolecular resolution of two- and three-dimensionally folded cytochrome c at surfaces. *Nano Lett.* **12**, 2452–8 (2012).
15. Clemmer, D. E., Hudgins, R. R. & Jarrold, M. F. Naked Protein Conformations: Cytochrome c in the Gas Phase. *J. Am. Chem. Soc.* **117**, 10141–10142 (1995).
16. Light-Wahl, K. J., Schwartz, B. L. & Smith, R. D. Observation of the Noncovalent Quaternary Associations of Proteins by Electrospray Ionization Mass Spectrometry. *J. Am. Chem. Soc.* **116**, 5271–5278 (1994).
17. Kreuzer, H. J., Nakamura, K., Wierzbicki, A., Fink, H. W. & Schmid, H. Theory of the point-source electron-microscope. *Ultramicroscopy* **45**, 381–403 (1992).
18. Latychevskaia, T., Longchamp, J.-N., Escher, C. & Fink, H.-W. Holography and coherent diffraction with low-energy electrons: A route towards structural biology at the single molecule level. *Ultramicroscopy* (2014). doi:10.1016/j.ultramic.2014.11.024
19. Latychevskaia, T. & Fink, H.-W. Practical algorithms for simulation and reconstruction of digital in-line holograms. *Appl. Opt.* **54**, 2424 (2015).
20. Heck, A. J. R. Native mass spectrometry: a bridge between interactomics and structural biology. *Nat. Methods* **5**, 927–933 (2008).
21. Laganowsky, A., Reading, E., Hopper, J. T. S. & Robinson, C. V. Mass spectrometry of intact membrane protein complexes. *Nat. Protoc.* **8**, 639–51 (2013).

22. Mehmood, S., Allison, T. M. & Robinson, C. V. Mass spectrometry of protein complexes: from origins to applications. *Annu. Rev. Phys. Chem.* **66**, 453–74 (2015).
23. Longchamp, J.-N., Latychevskaia, T., Escher, C. & Fink, H.-W. Graphene Unit Cell Imaging by Holographic Coherent Diffraction. *Phys. Rev. Lett.* **110**, 255501 (2013).
24. Pauly, M. *et al.* A hydrodynamically optimized nano-electrospray ionization source and vacuum interface. *Analyst* **139**, 1856–67 (2014).
25. Gabor, D. A new microscopic principle. *Nature* **161**, 777–778 (1948).
26. Gabor, D. Microscopy by reconstructed wave-fronts. *Proc. R. Soc. London Ser. A - Math. Phys. Sci.* **197**, 454–487 (1949).
27. Fink, H. W. Point-source for ions and electrons. *Phys. Scr.* **38**, 260–263 (1988).
28. Stocker, W., Fink, H. W. & Morin, R. Low-energy electron and ion projection microscopy. *Ultramicroscopy* **31**, 379–384 (1989).
29. Kahle, S. *et al.* The Quantum Magnetism of Individual Manganese-12-Acetate Molecular Magnets Anchored at Surfaces. *Nano Lett.* **12**, 518–521 (2012).
30. Kley, C. S. *et al.* Atomic-scale observation of multiconformational binding and energy level alignment of ruthenium-based photosensitizers on TiO<sub>2</sub> anatase. *Nano Lett.* **14**, 563–9 (2014).

#### **Acknowledgements:**

We would like to thank Frank Sobott and Ester Martin for advice on preparing native protein beams. The work presented here is financially supported by the Swiss National Science Foundation (SNF). We also appreciate support by the EU commission for building the equipment in the frame of the former SIBMAR project.

#### **Authors Contribution:**

J.-N. L. had the original idea to combine ES-IBD and low-energy electron holography and further elaborated the concept with K.K and H.-W.F. J.-N. L. prepared the ultraclean freestanding graphene supports and recorded the holograms. S.R. and J.-N. L. planned the deposition experiments and along with S.A. performed the electrospray deposition of the proteins onto graphene. T.L. performed the hologram reconstructions with her self-developed software package. S.R. and J.-N. L. interpreted the data. H.-W. F. invented the technology of lens less holography with low-energy electrons based on atomic sized coherent electron point sources. C.E., T.L., J.-N. L., & H.-W. F. further developed the low-energy electron holographic microscope used in this study. S.R. and K.K. developed the ES-IBD technique. J.-N. L, C. E. & H.-W. F. wrote the manuscript main text and with S.R the supplementary information, in discussions with all remaining authors.

#### **Methods:**

Ultraclean freestanding graphene is prepared by the Pt-metal catalysis method described in detail elsewhere<sup>6</sup>. Prior to the transfer of the ultraclean substrate from the UHV chamber of the low-energy electron holographic microscope to the UHV chamber of the ES-IBD device, the cleanliness of the substrate is characterized and reference images are recorded for comparing the very same region of freestanding graphene before and after protein deposition.

During the whole experimental workflow, the samples are kept under strict UHV conditions with the help of a UHV suitcase for transfer between the two experimental chambers. Details of the ES-IBD procedure and of the low-energy electron holography experimental scheme are described in the supplementary information document.

## Supplementary Information

### 1. ES-IBD

Soft-landing electrospray ion beam deposition takes place in a home-built instrument<sup>4,5</sup>. The ion beam is generated by a nano electrospray source with an optimized hydrodynamic behaviour<sup>24</sup> at a flow rate of 20-30 $\mu$ L/h and an emitter voltage of approximately 3kV. The positive ions enter the vacuum through a heated metal capillary and are collimated in an ion funnel and a collisional collimation quadrupole operated in *rf*-only mode. In the third pumping stage a mass filtering quadrupole selects the *m/z* region of interest, which is monitored by the time-of-flight mass spectrometer in the fourth pumping stage. Here, a retarding field energy analyser measures the kinetic energy of the ions. The beam is then guided by electrostatic lenses towards the target in the 6<sup>th</sup> pumping stage being at 2 $\times$ 10<sup>-10</sup>mbar, where the protein deposition takes place. To ensure gentle landing, the collision energy is controlled by applying a bias voltage to the target and hence reducing the kinetic energy of the protein ions.

To obtain ion beams of native CytC (bovine, Fluka 30398), a solution of 0.15mg/mL was prepared in aqueous 50mM ammonium acetate buffer. With a spray flow rate of 25 $\mu$ L/hr, an ion current of 1.1nA is detected at the TOF-MS. Unfiltered mass spectra (Fig. S1 left/top) show low charge states of +5 to +7, corresponding to folded CytC. At lower *m/z* values peaks corresponding to highly charged (*z*>+8) unfolded CytC and peaks that relate to fragments or contamination are found. Note that, due to the limited dynamic range of the TOF-MS, the detector amplification was set very high, such that the peaks of the native CytC are distorted. The *m/z* selective quadrupole was tuned to select a *m/z*-window from 1250u/e to approximately 3500u/e by setting a *rf*-amplitude of 700V with a differential dc-voltage of 5%. This results in a beam of predominantly native CytC (Fig. S1 left/bottom) from which unfolded proteins (low *m/z*) and undefined heavy aggregates (high *m/z*) are removed.

Haemoglobin (bovine, Sigma H2500) is a protein complex of four myoglobin subunits, two A and two B. Ion beams are generated from solutions of 0.3mg/mL HG prepared in 50mM ammonium acetate buffer. A current of 600pA is detected at the TOF-MS. The mass spectrum is very complex and is resolved only partially due to the limited performance concerning resolution and dynamic range of the home-built linear TOF-MS. Nevertheless, a comparison with literature spectra allows identifying characteristic peaks (Fig. S1 right/bottom), which become more pronounced after removal of the unspecific agglomeration in the high *m/z* range (>5000u/e) by mass filtering with the quadrupole. The beam transmitted for deposition contains native intact HG complexes (Q<sup>17+</sup>, Q<sup>16+</sup>) along with dimers (D) and monomers (HBA).



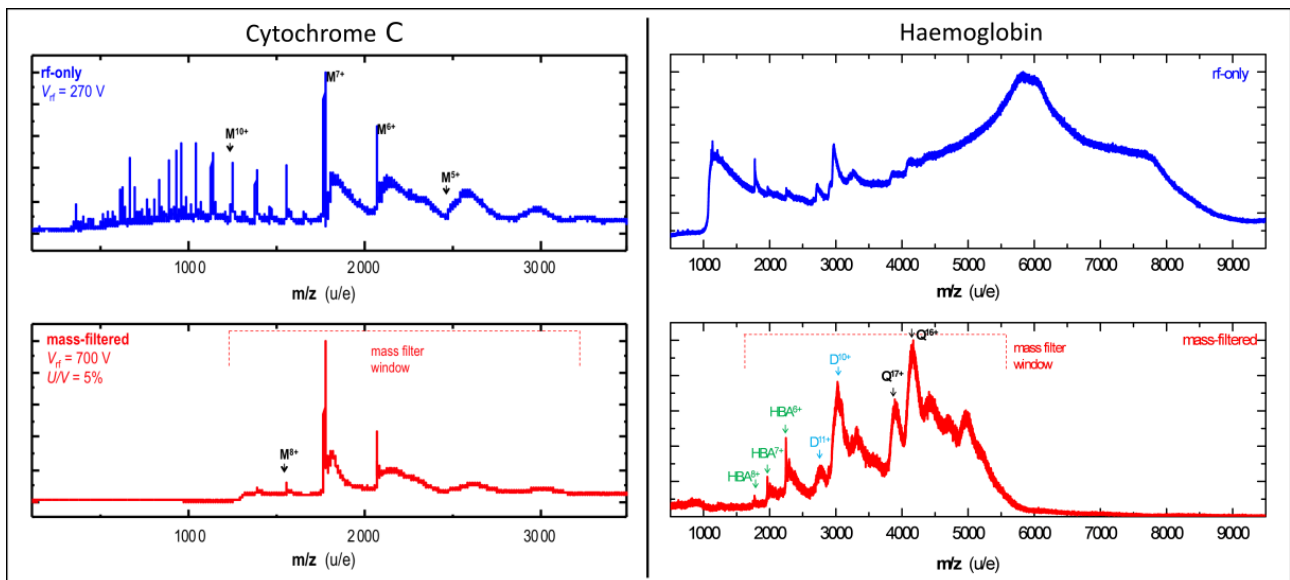


Fig. S1: Mass spectra of Cytochrome C (left) and Haemoglobin (right). Top: the  $m/z$  spectra before mass filtering are displayed. Bottom: the corresponding mass-filtered spectra.

## 2. Low-Energy Electron Holography

In the low-energy electron holographic setup<sup>3</sup>, inspired by Dennis Gabor's original idea of in-line holography<sup>25,26</sup>, a sharp (111)-oriented tungsten tip acts as electron point source (EPS) providing a divergent beam of highly coherent electrons<sup>27,28</sup>. The atomic sized electron field emitter can be brought as close as 100nm to the sample with the help of a 3-axis nanopositioner. Part of the electron wave is elastically scattered off the object and hence is called the object wave, while the un-scattered part of the wave represents the reference wave. At a distant detector, the hologram, i.e. the pattern resulting from the interference of these two wave fronts is recorded. The magnification of the imaging system is given by the ratio between detector-to-source distance and sample-to-source distance and can be as high as  $10^5$ . A hologram, in contrast to a diffraction pattern, contains the phase information of the object wave, and the object structure can thus be reconstructed unambiguously. The numerical reconstruction from the hologram is essentially achieved by back propagation to the object plane, which corresponds to evaluating the Fresnel-Kirchhoff integral transformation<sup>17-19</sup>.

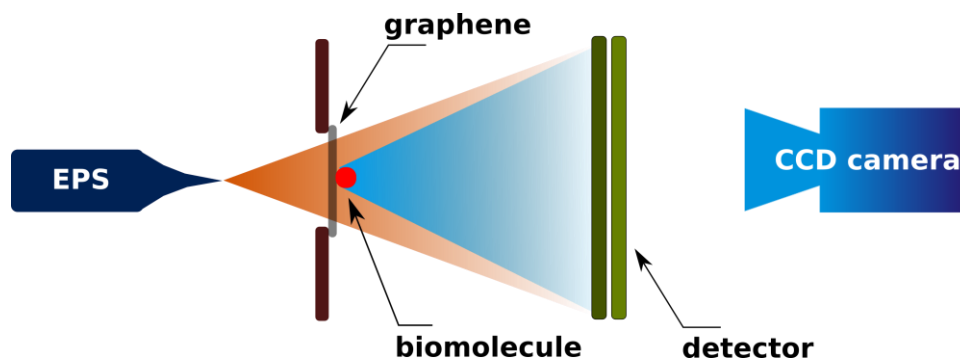


Fig. S2: Low-Energy Electron Holography Scheme

### 3. UHV Transfer

A vacuum suitcase, Fig. S3(a) (*Ferrovac GmbH, Zurich*), is used to transfer samples between the two UHV based experiments, electron holography on the one side, and electrospray ion beam deposition on the other side.

The suitcase is equipped with a SAES getter/ion getter pump combination operated by a battery driven power supply. The pressure is kept below  $2 \times 10^{-10}$  mbar at all times, except for the short duration of the transfer (1-2 minutes) where it rises into the  $1 \times 10^{-9}$  mbar regime. The performance of this suitcase, originally developed for STM experiments is well known from various surface science studies<sup>29,30</sup>.

Each instrument is equipped with a load-lock to which the suitcase can be attached. The load-lock is pumped by a turbo molecular pump supported by a cryogenic active charcoal trap at LN<sub>2</sub> temperature. A pressure in the  $10^{-9}$  mbar range is established within a few hours, ensuring a contamination-free transfer of the samples. Figure S3 shows low-energy electron projection images of the very same freestanding graphene region before (b) and after (c) the transfer from the low-energy electron holographic microscope located in Zurich to the ES-IBD chamber in Stuttgart and back to the microscope in Zurich. No relevant sign of contamination due to transfer and transport is observed.

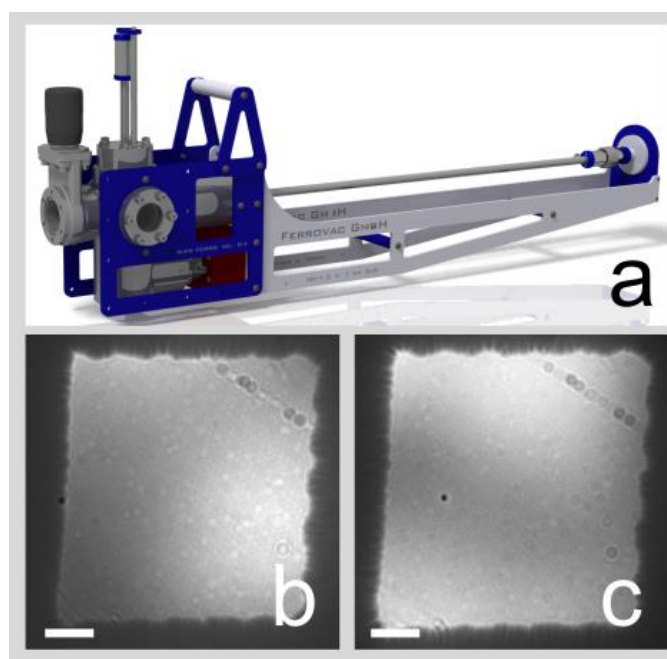


*Fig. S3: UHV Vacuum Suitcase and its performance. **a**, Three-dimensional rendering of the transport suitcase enabling UHV transfer of ultraclean freestanding graphene between the low-energy electron microscope and the ES-IBD chamber. Low-energy electron projection images before (**b**) and after (**c**) a complete transfer and travel cycle without protein deposition. During the course of the transfer procedure between the two vacuum chambers no relevant contamination of the graphene built up.*

## Extended Data Figures

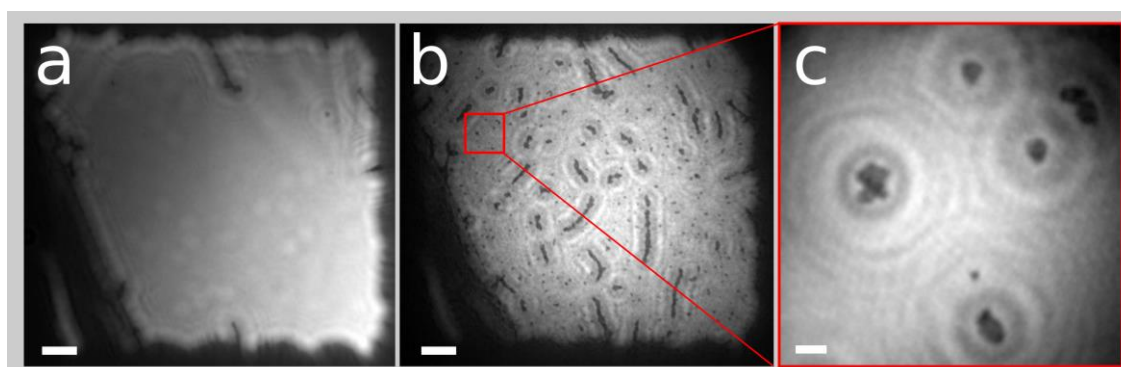


*Fig. Extended Data 1: Freestanding graphene before (a) and after (b) the deposition of 30pA/h native CytC. In b individual globular objects of a size of 2-5nm or agglomerates thereof are observed. Such agglomeration has previously been observed on a Au(111) surface after deposition of native CytC in low charge states<sup>14</sup>. c, After moving the electron point source closer to the globular objects, their dimensions can be measured and correspond to the size of individual folded CytC molecules. The scale bars correspond to 50nm in a and b and to 5nm in c.*

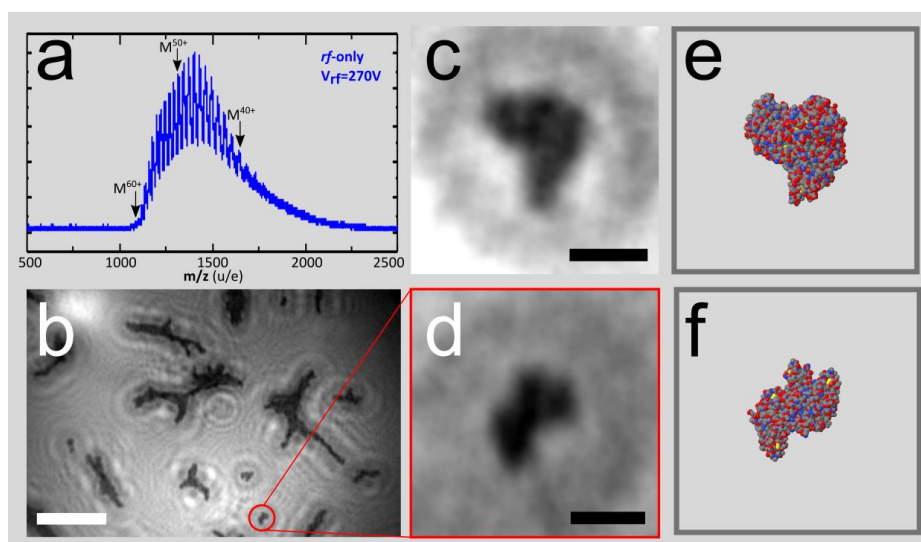


*Fig. Extended Data 2: Images of individual BSA proteins deposited onto freestanding graphene. a, Mass spectrum of the BSA ion beam. Ion beams of mainly unfolded BSA (Sigma A4919) were prepared by electrospraying solutions of 0.4mg/mL BSA dissolved in a 1:1 mixture of water and ethanol to which 2% formic acid is added. At a flow rate of 30 $\mu$ L/hr, an ion current of 2nA is measured at the TOF-MS. The mass spectrum above 1000u/e shows the characteristic peak group of multiply charged proteins ( $z = +35 \dots +60$ ). The low  $m/z$  range (<1000u/e) as well as the high  $m/z$  range (>2000 u/e) is free of any peaks indicating a pure beam free of contamination and unspecific agglomerations. b, Survey image of the deposited high-charge state BSA proteins on graphene. As expected from the mass spectrum the vast majority of proteins are in an unfolded state. Two high magnification images of BSA in a folded structure are presented in c and d. The scale bars correspond to 50nm in b and 5nm in c and d. The atomic model of BSA from the protein data bank (pdb id: 3V03) in the corresponding orientations is displayed in e and f for comparison.*

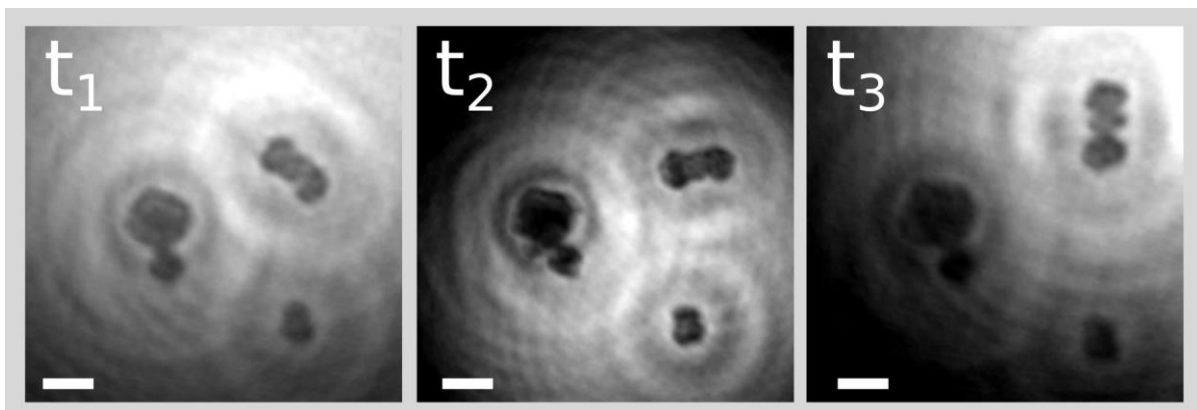


*Fig. Extended Data 3: Time evolution of the orientation of CytC complexes. The time lapse between subsequent observations amounts to 30sec. From these images it is evident that at least some of the deposited proteins are mobile on freestanding graphene. Low-energy electron holography appears to be a method for also studying diffusion of proteins on surfaces. This observation suggests that a low-energy electron holographic microscope operating at cryogenic temperatures might be needed in order to fix the protein in space and attain atomic resolution. The scale bars correspond to 5nm.*